USGS

InSAR imaging of Aleutian Volcanoes

Zhong Lu

SAIC, USGS/EROS
Sioux Falls, SD 57198
lu@usgs.gov
http://edc.usgs.gov/Geo_Apps

Acknowledgements:
- Contributions by many colleagues.
- Funding from NASA, USGS LRS Program, USGS Director Venture Capital Funds, USGS Volcano Hazards Program, USGS Earthquake Hazards Program, and NSF.
- SAR imagery from ASF, ESA, and JAXA.

USGS

Outline

- Introduction to InSAR
- Issues on InSAR processing
- InSAR imaging of Aleutian volcanoes
  - Okmok
  - Seguam
- A few thoughts

USGS

Radar is an instrument for measuring distance

- In its simplest form, a radar operates by broadcasting a pulse of electromagnetic energy into space – if that pulse encounters an object then some of that energy is redirected back to the radar antenna.
- Precise timing of the echo delays allows determination of the distance, or "range", while measuring the Doppler frequency tells the velocity of the target.

USGS

Synthetic aperture radar is an active microwave sensor

- The electromagnetic wave is transmitted from the satellite. The wave propagates through the atmosphere, interacts with the Earth surface. Part of the energy is returned back and recorded by the satellite.
- By sophisticated image processing technique, both the intensity and phase of the reflected (or backscattered) signal can be calculated. So, essentially, a complex-valued SAR image represents the reflectivity of the ground surface.
- The amplitude or intensity of the SAR image is primarily controlled by terrain slope, surface roughness, and dielectric constants, while the phase of the SAR image is primarily controlled by the distance from satellite antenna to ground targets and partially controlled by the atmospheric delays as well as the interaction of microwave with ground surface.

USGS — How Radar Interferometry Works

- Traditionally, distance measurement is done by precise timing.
- Accuracy is several meters for spaceborne sensor.

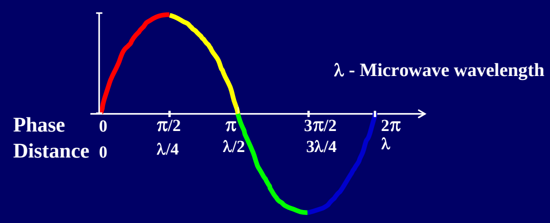

- In interferometry, the distance from the satellite to the ground is achieved by measuring the phase of the electromagnetic wave.
- Accuracy is about centimeter to sub-centimeter.

USGS — How InSAR Works

- Interferometric synthetic aperture radar (InSAR) combines phase information from two or more radar images of the same area acquired from similar vantage points at different times to produce an interferogram.
- The interferogram, depicting range changes between the radar and the ground, can be further processed with a digital elevation model (DEM) to image ground deformation at a horizontal resolution of tens of meters over areas of ~100 km x 100 km with centimeter to sub-centimeter precision under favorable conditions.

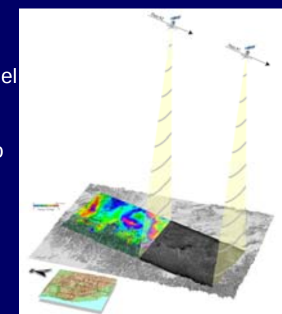

USGS — Step 1 - Two SAR images

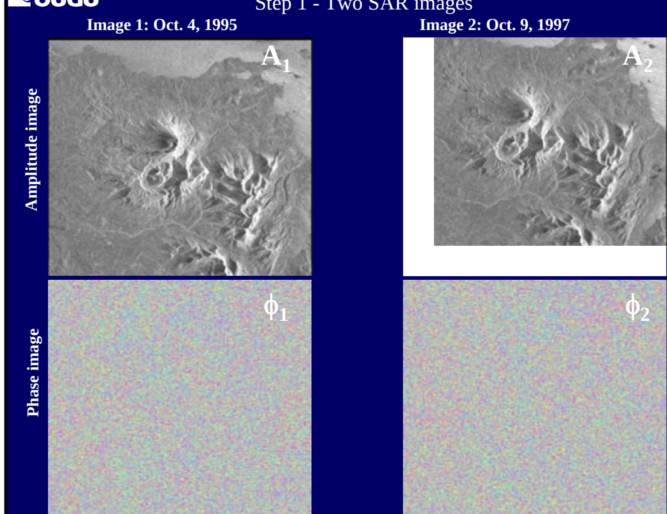

Images are about 28 km by 25 km

USGS — Step 2 - SAR images are co-registered

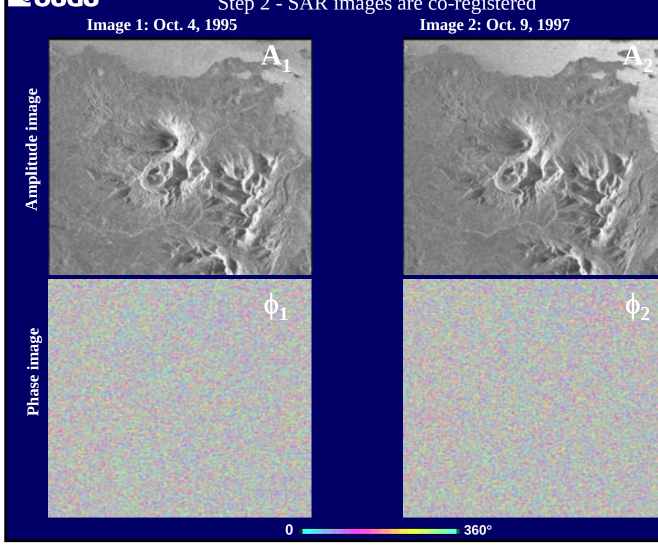

USGS

Step 3 - Original interferogram: $\Delta\phi_{init} = \phi_1 - \phi_2$

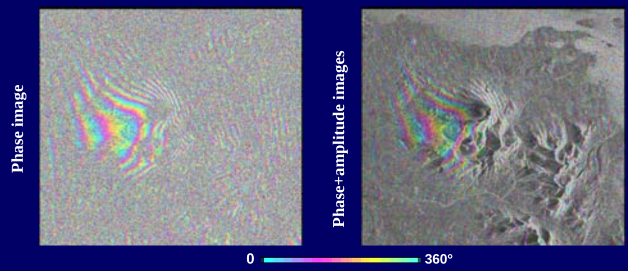

USGS

Step 4 - Phase difference caused by difference of satellite positions over a flat earth: $\Delta\phi_{flat}$

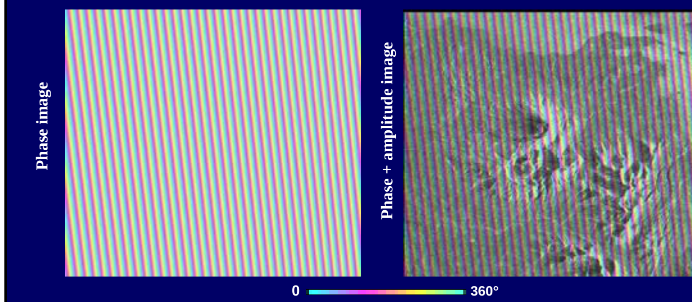

USGS

Step 5 - Flattened interferogram: $\Delta\phi_{init} - \Delta\phi_{flat}$

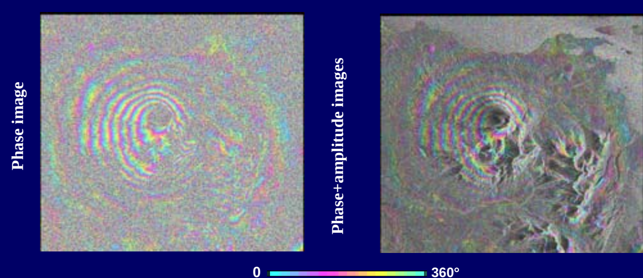

USGS

Step 6 - Topography-only interferogram: $\Delta\phi_{topo}$

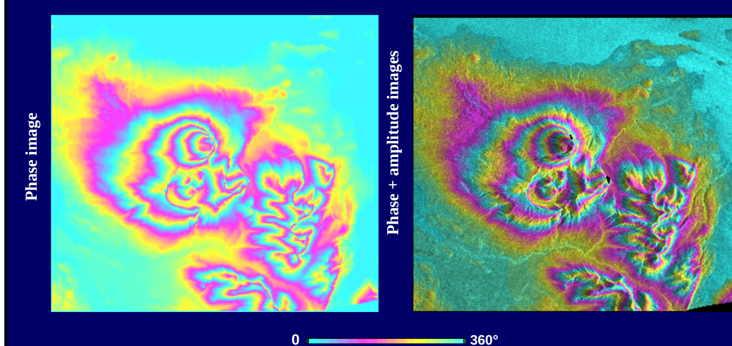

Step 7 - Deformation interferogram (+noise):

$$\Delta\phi_{def} = \Delta\phi_{init} - \Delta\phi_{flat} - \Delta\phi_{topo}$$

Phase image

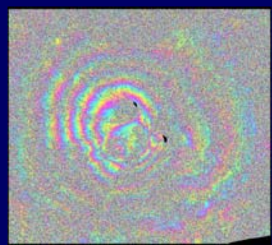

Phase+amplitude images

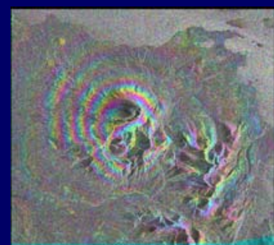

0 2.83 cm

Step 8 - Deformation interferogram with noise reduction:

$$\Delta\phi_{def} = \Delta\phi_{init} - \Delta\phi_{flat} - \Delta\phi_{topo}$$

Filtered phase image

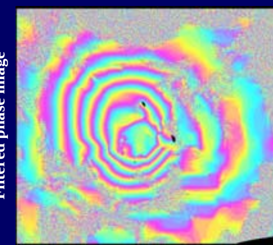

Filtered phase + Intensity images

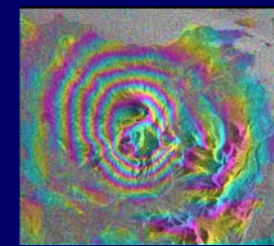

0 2.83 cm

Step 9 - Deformation interferogram in map projection

Phase image draped over an amplitude image

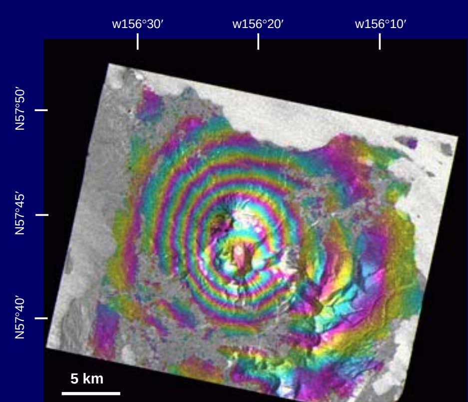

0 2.83 cm

Step 9 - Deformation interferogram in map projection

Phase image draped over a DEM image

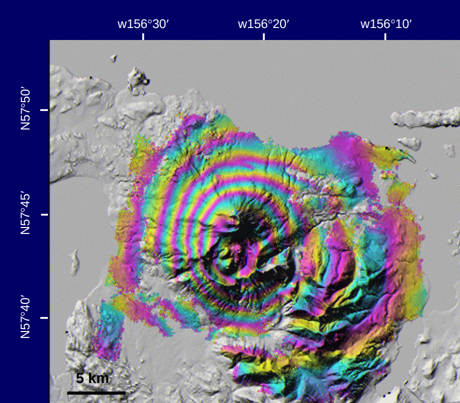

0 2.83 cm

USGS

Step 10 – Deformation interpretation

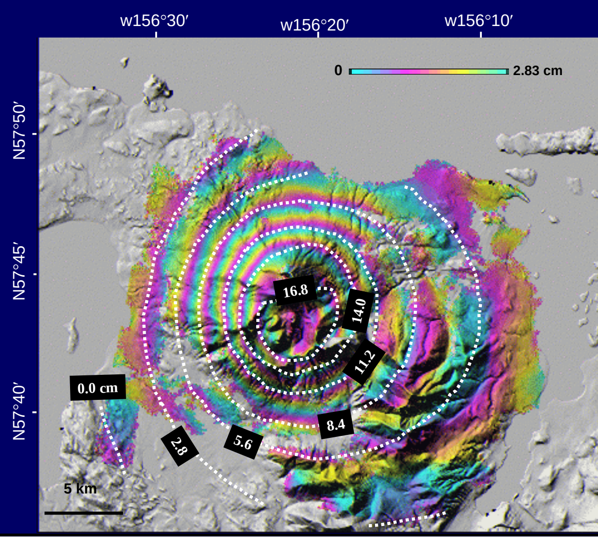

USGS

Representation of Interferometric Data

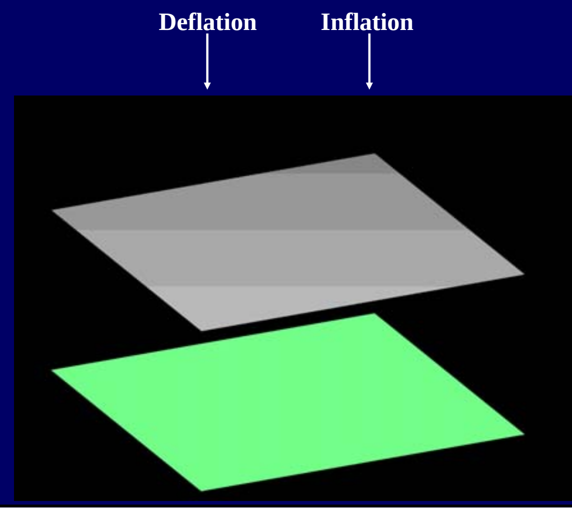

USGS

Step 11 - Deformation modeling

4 Oct. 95 - 9 Oct. 97

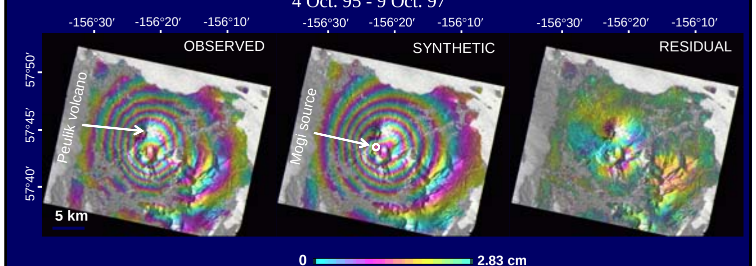

Best-fit source parameters:
- The model source is located at a depth of 6.5 ± 0.2 km.
- The calculated volume change of magma reservoir is 0.043 ± 0.002 km^3.

USGS

Synthetic Aperture Radar Satellites

- Current and Past Sensors
  - European ERS-1, 1991-2000, C-band, 35-day repeat cycle
  - European ERS-2, 1995-now, C-band, 35-day repeat cycle (experiencing malfunctions since early 2001)
  - Japanese JERS-1, 1992-1998, L-band, 44-day repeat cycle
  - Canadian Radarsat-1, 1995-now, C-band, 24-day repeat cycle
  - European Envisat, 2002-now, C-band, 35-day repeat cycle
- Future Sensors
  - Japanese ALOS, 2006, L-band, 46-day repeat cycle
  - Canadian Radarsat-2, 2006(?), C-band
  - German TerraSAR-X, 2006(?), X-band
  - U.S. DOD Space-based Radar Constellations
  - U.S. ECHO+, forever?
  - Chinese SAR Constellation (5 satellites), next decade
  - …

Wavelength (λ)
- X-band: λ = ~3 cm
- C-band: λ = ~5.7 cm
- L-band: λ = ~24 cm

USGS Interferometric Synthetic Aperture Radar (InSAR)

- Errors in InSAR observations
  - Temporal decorrelation of ground surface due to dense vegetation and other environmental changes – Wavelength dependence.
  - Atmospheric delay anomalies
  - Artifacts due to uncertainties in determining satellite positions

SOLUTIONS →

- Observations from independent images
- Interferometric permanent scattering technique
- Longer wavelength radar
- Shorter visit cycle

USGS Atmospheric artifacts

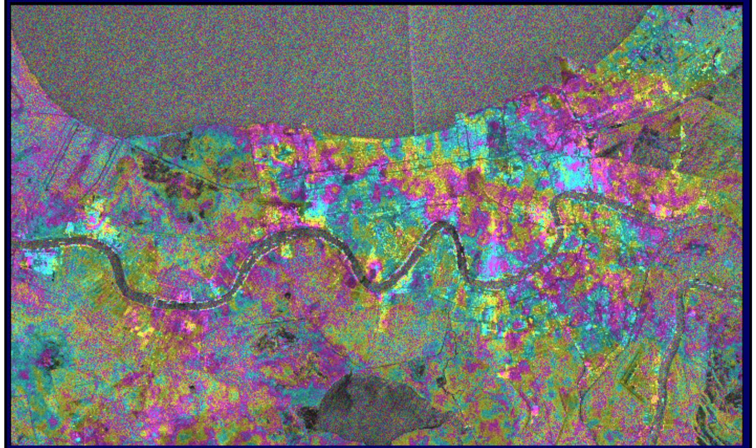

range change
0 2.83 cm

1995/09/18 – 1995/09/19

USGS Atmospheric artifacts

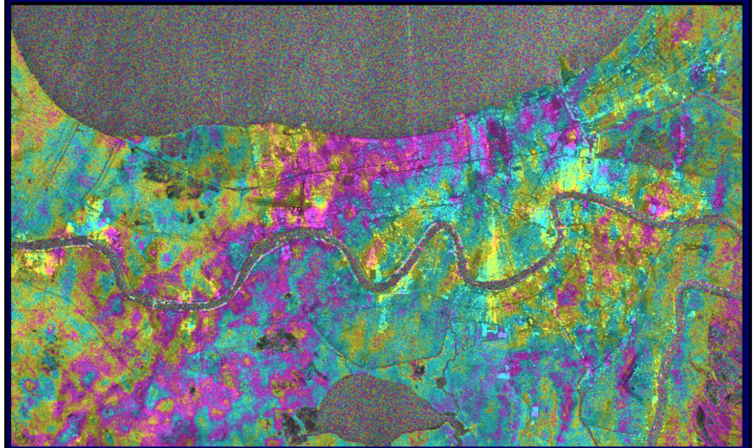

range change
0 2.83 cm

1995/11/27 – 1995/11/28

USGS Deformation of New Orleans

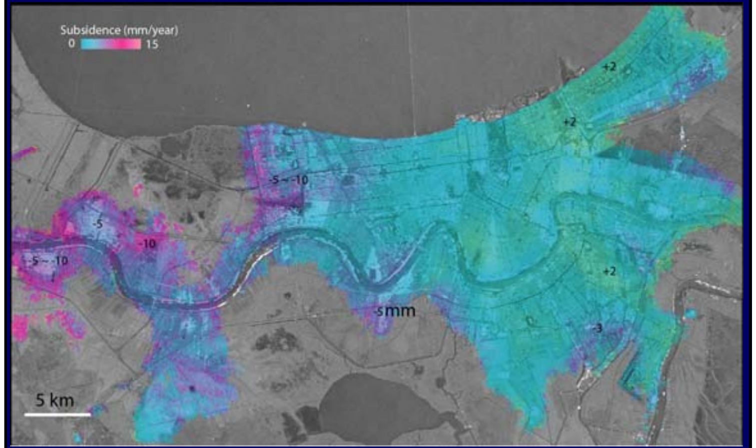

Very preliminary result – no quote or citation

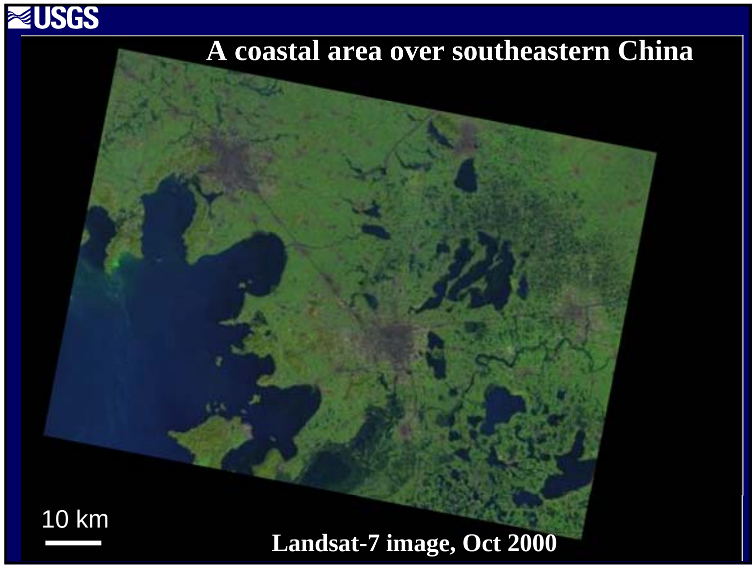
USGS
A coastal area over southeastern China
10 km
Landsat-7 image, Oct 2000

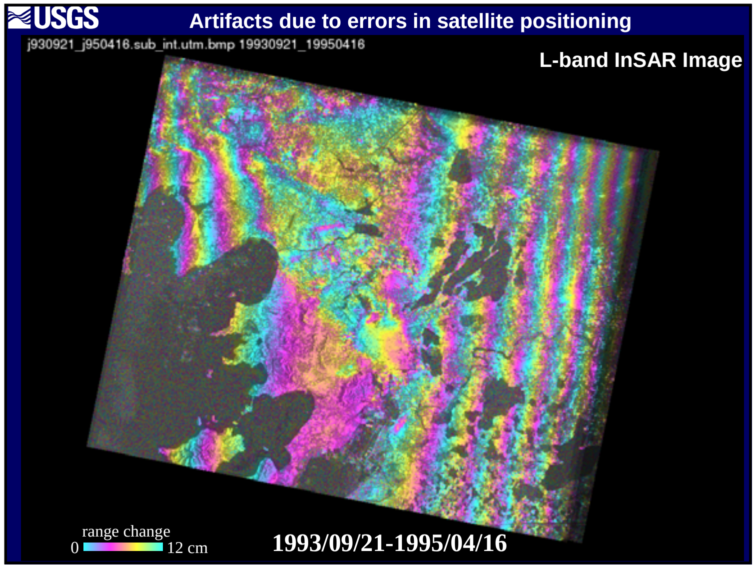
USGS
Artifacts due to errors in satellite positioning
j930921_j950416.sub_int.utm.bmp 19930921_19950416
L-band InSAR Image
range change
0 12 cm
1993/09/21-1995/04/16

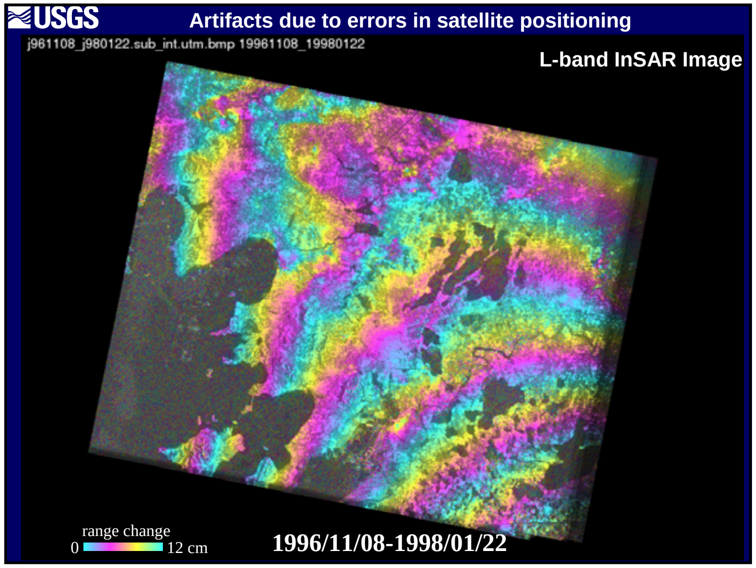
USGS
Artifacts due to errors in satellite positioning
j961108_j980122.sub_int.utm.bmp 19961108_19980122
L-band InSAR Image
range change
0 12 cm
1996/11/08-1998/01/22

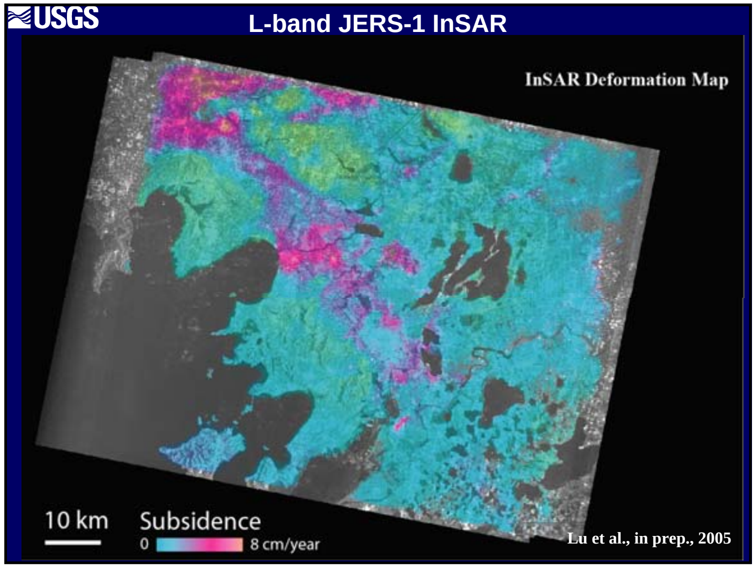
USGS
L-band JERS-1 InSAR
InSAR Deformation Map
10 km
Subsidence
0 8 cm/year
Lu et al., in prep., 2005

USGS

Subsidence was up to 8 cm/year

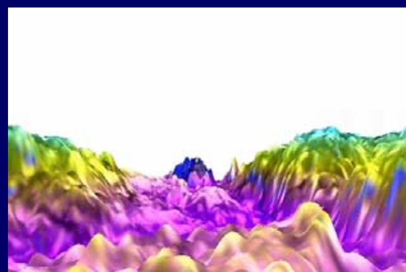

Land subsidence + GIS data layers over cities provide critical information for decision making

USGS

Precise mapping of surface deformation is a critical element in the assessment and mitigation of hazardous events.

- Mapping surface subsidence and uplift related to extraction and injection of fluids in groundwater aquifers and petroleum reservoirs provides fundamental data on reservoir/aquifer properties and processes and improves our ability to assess and mitigate undesired consequences.
- Monitoring dynamic water-level changes beneath wetlands can improve hydrological modeling predictions and enhance the assessment of future flood events over wetlands.
- Measuring spatial and temporal patterns of surface deformation in seismically active regions are extraordinarily useful for estimating seismic risks and improving earthquake predictions.
- Measuring and documenting how landslides develop and are activated are prerequisites to minimize the hazards they pose in areas of rapid urban growth.
- Measuring how a volcano's surface deforms before, during and after eruptions provides essential information about magma dynamics and a basis for mitigating volcanic hazards.

USGS

InSAR imaging of Aleutian Volcanoes

USGS

Aleutian Arc Volcanoes

InSAR Survey of Alaskan Volcanoes

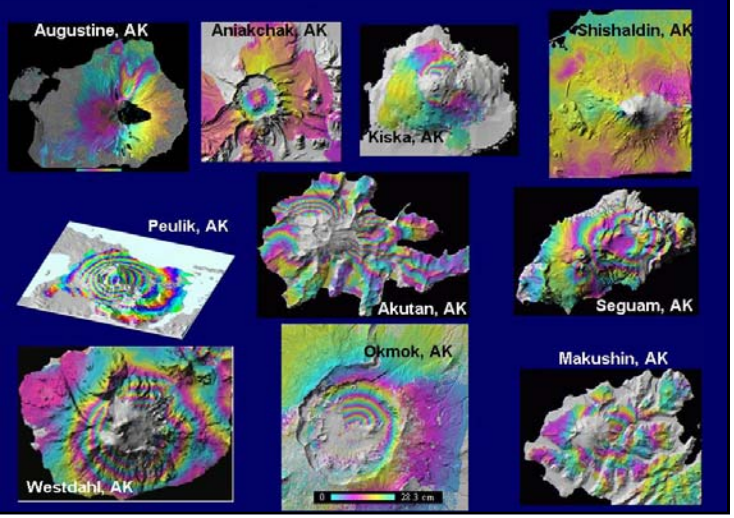

Okmok Volcano

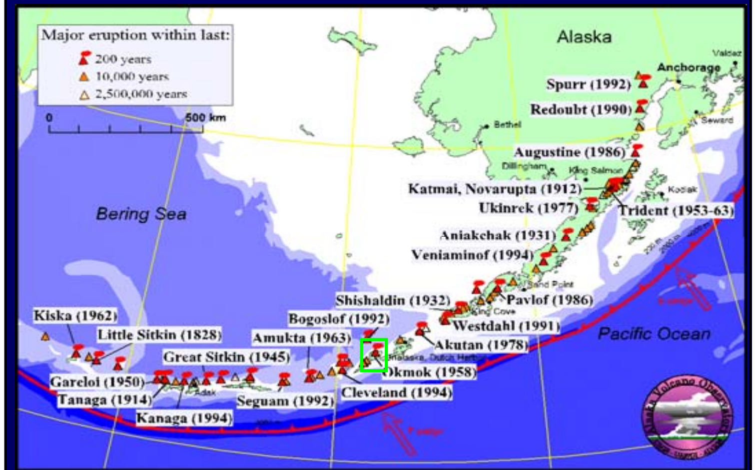

Okmok Volcano

Facts about Okmok

- Shield volcano
- Caldera formed 2050 years ago
- ~10 minor explosive eruptions (ash) in 20th century
- 3 large effusive eruptions (basaltic flows) in 1945, 1958 and 1997
- All eruptions from Cone A

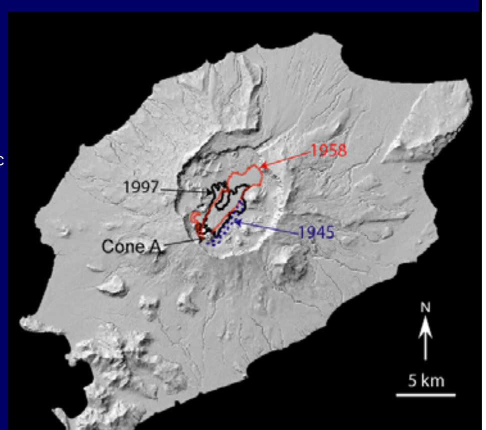

Estimating Lava Flow Volume of 1997 Eruption

1. The pre-eruption DEM is produced using repeat-pass ERS InSAR data; multiple interferograms are combined to reduce errors due to atmospheric variations, and deformation rates are estimated independently and removed from the interferograms used for DEM generation.

2. Post-eruption DEM is generated from airborne (TOPSAR) InSAR images where a three-dimensional affine transformation is used to account for the misalignments between different DEM patches.

USGS

Interferograms used for DEM generation

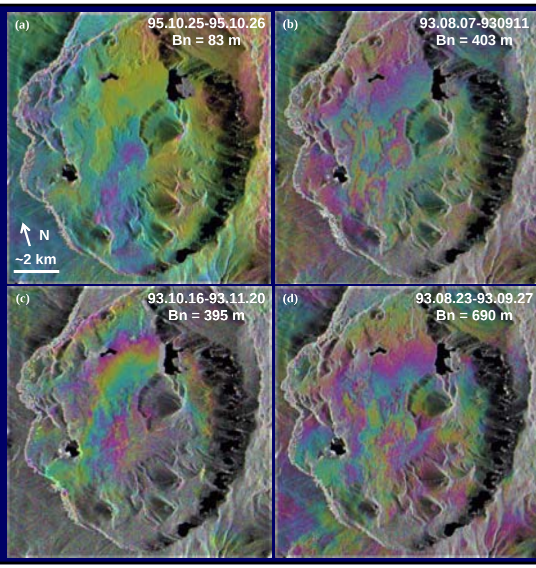

USGS

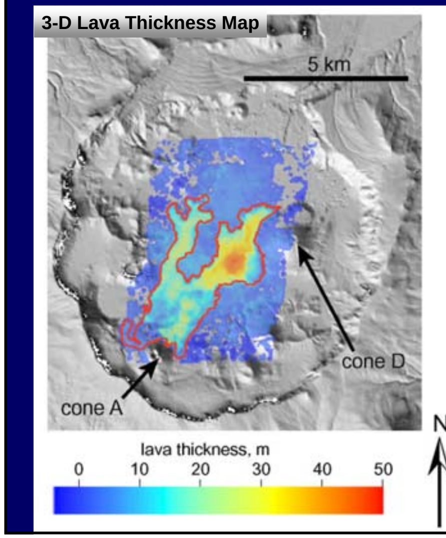

- **T**hickness is heterogeneous.
- The thickest portion of the lava reaches to 50 m, while field measurements at lava edges never exceed 20m.
- Eruption volume is about 0.154 km^3.

USGS

Lava thickness derived from the difference of pre-eruption and post-eruption DEMs

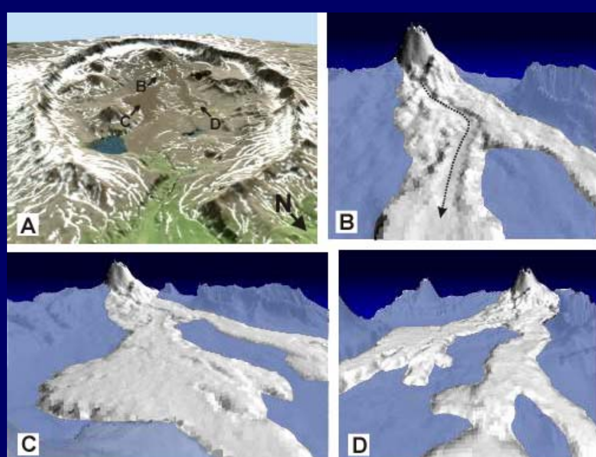

Lu et al., 2003; Patrick et al., 2003

USGS

AVHRR Thermal Observations Confirmed Lava Thickness

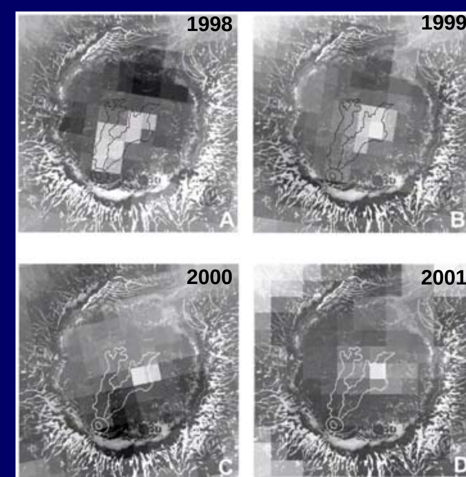

Courtesy of K. Papp

Multi-temporal AVHRR thermal images draped over Landsat-7 Band-8 image

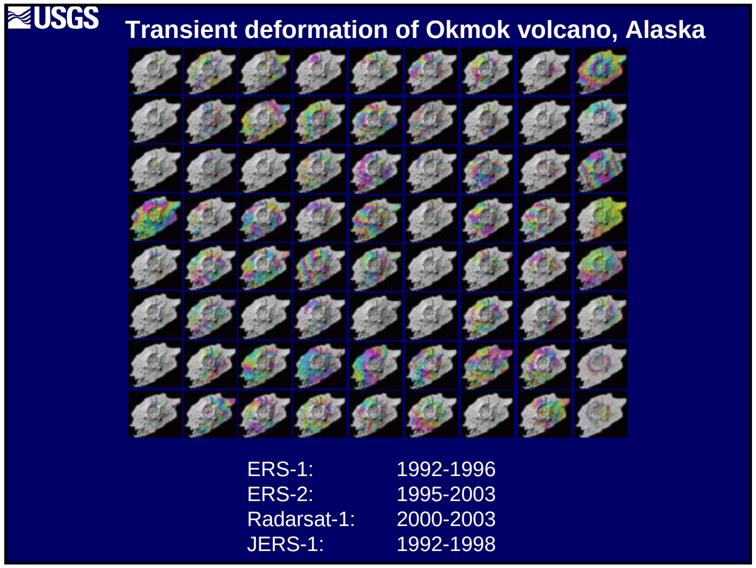
USGS
Transient deformation of Okmok volcano, Alaska
ERS-1: 1992-1996
ERS-2: 1995-2003
Radarsat-1: 2000-2003
JERS-1: 1992-1998

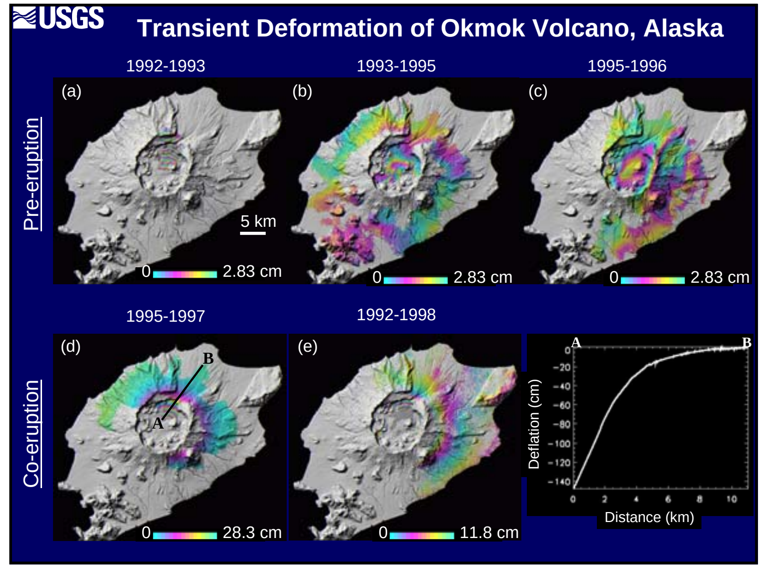
USGS
Transient Deformation of Okmok Volcano, Alaska
1992-1993
1993-1995
1995-1996
Pre-eruption
(a)
(b)
(c)
5 km
0 2.83 cm
1995-1997
1992-1998
Co-eruption
(d)
(e)
0 28.3 cm
0 11.8 cm
Deflation (cm)
Distance (km)

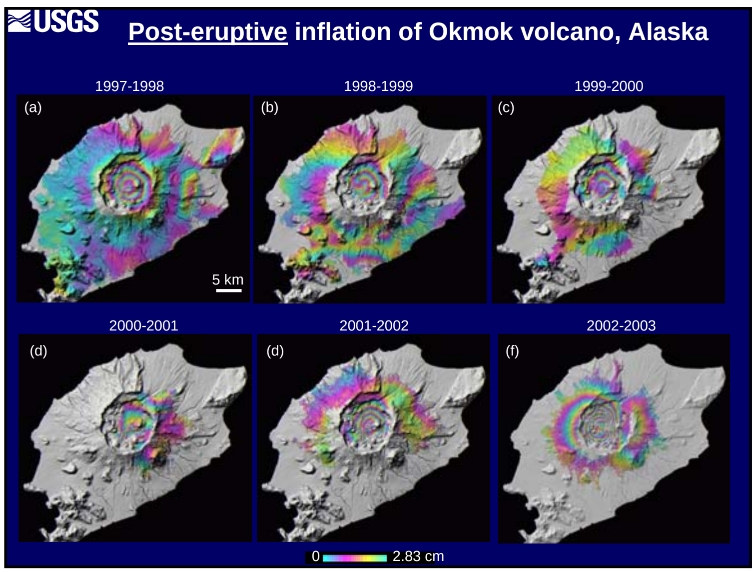
USGS
Post-eruptive inflation of Okmok volcano, Alaska
1997-1998
1998-1999
1999-2000
(a)
(b)
(c)
5 km
2000-2001
2001-2002
2002-2003
(d)
(d)
(f)
0 2.83 cm

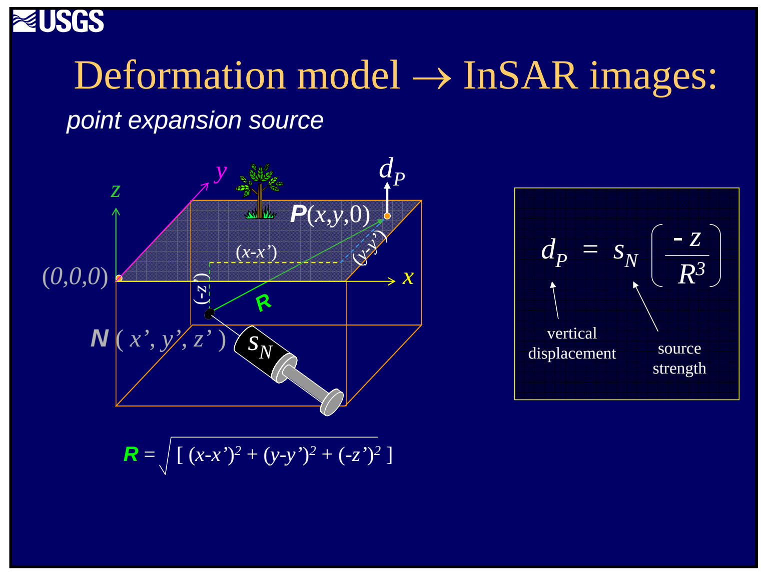
USGS
Deformation model → InSAR images:
point expansion source
z
y
x
d_P
P(x,y,0)
(0,0,0)
(x-x')
(y-y')
(-z')
R
N (x', y', z')
s_N
$d_P = s_N \left(\frac{-z}{R^3} \right)$
vertical displacement
source strength
$R = \sqrt{[\,(x-x')^2 + (y-y')^2 + (-z')^2\,]}$

USGS — Magma supply rate for the shallow reservoir

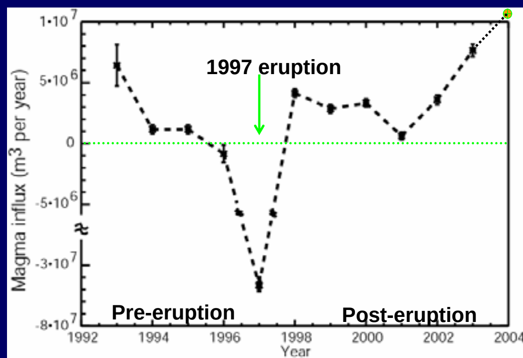

- A magma reservoir residing at 3.2 km beneath the center of the caldera, is responsible for the observed deformation before, during and after the 1997 eruption.
- By the summer of 2004, 45~75% of the magma volume from the 1997 eruption had been replenished.

USGS — Deformation of lava flows erupted before 1997

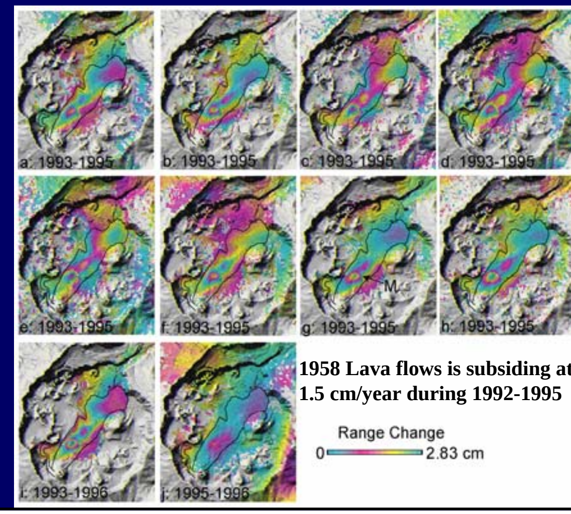

USGS — Deformation of lava flows after 1997 eruption

C-band Images

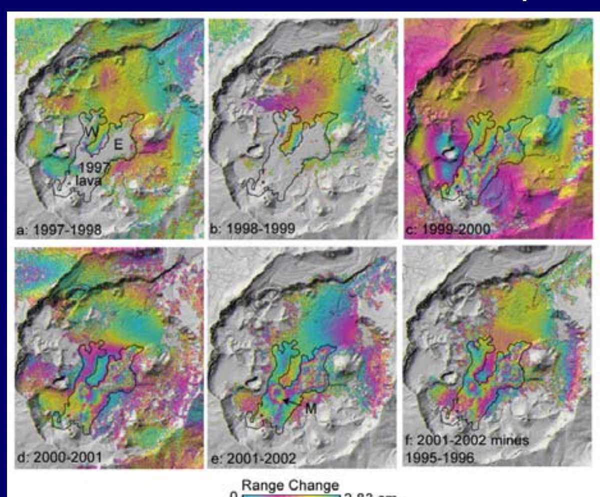

USGS — Deformation of 1997 lava flows from JERS-1 Imagery

L-band Images

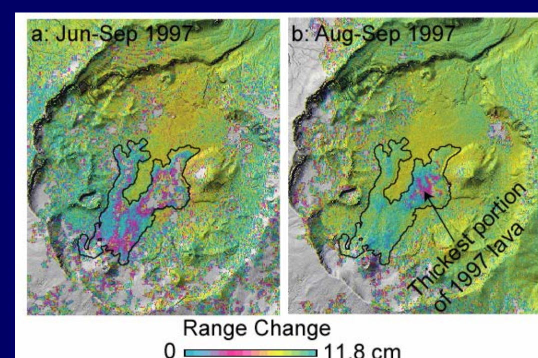

Surface displacement due to lava contraction and consolidation can be 2 mm/day or more four months after the emplacement

Deformation fields of Okmok volcano

Interferograms after the 1997 eruption suggest at least four distinct deformation processes:

1. volcano-wide inflation due to replenishment of the shallow magma reservoir,
2. subsidence of the 1997 lava flows due to thermal contraction,
3. deformation of the 1958 lava flows due to loading by the 1997 flows, and
4. continuing thermal contraction of 1958 lava flows buried beneath 1997 flows.

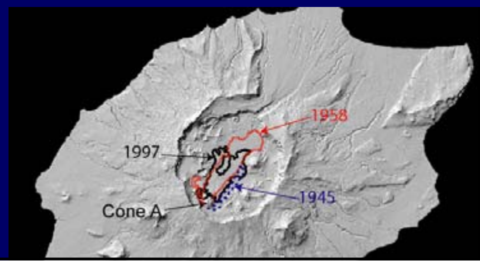

Transient volcano deformation sources imaged with InSAR: Application to Seguam island

Seguam Volcano, Alaska
- **Erupted in 1927 and 1977**
- **Last eruption: Dec. 27, 1992**
  May 28, 1993
  Jul. 31 – Aug. 19, 1993

Masterlark, T., and Z. Lu, JGR, 2004.

Seguam Volcano

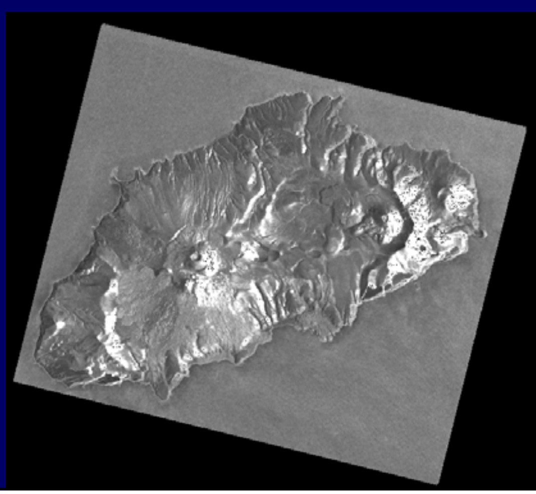

InSAR Images of Seguam Volcano

InSAR images of Seguam Volcano: 30 images document deformation during a variety of time intervals between 1992-2000.

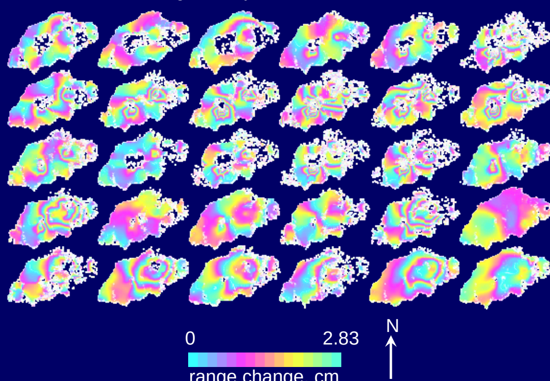

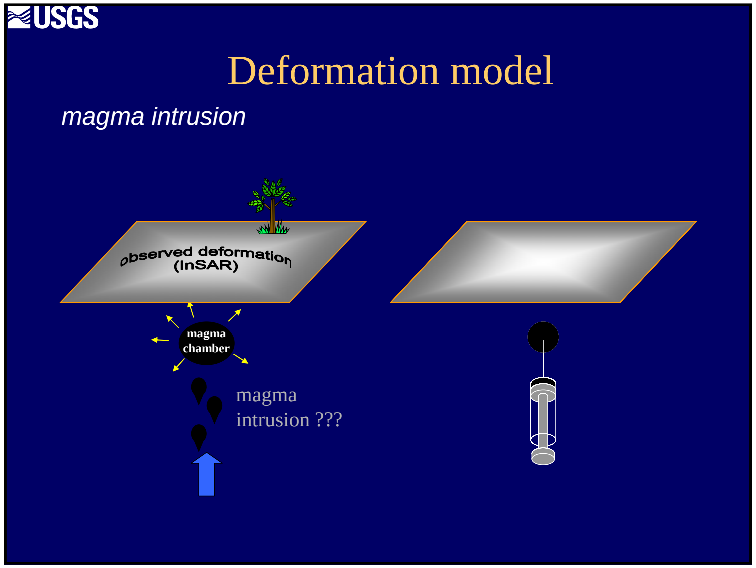
USGS
Deformation model
magma intrusion
observed deformation (InSAR)
magma chamber
magma intrusion ???

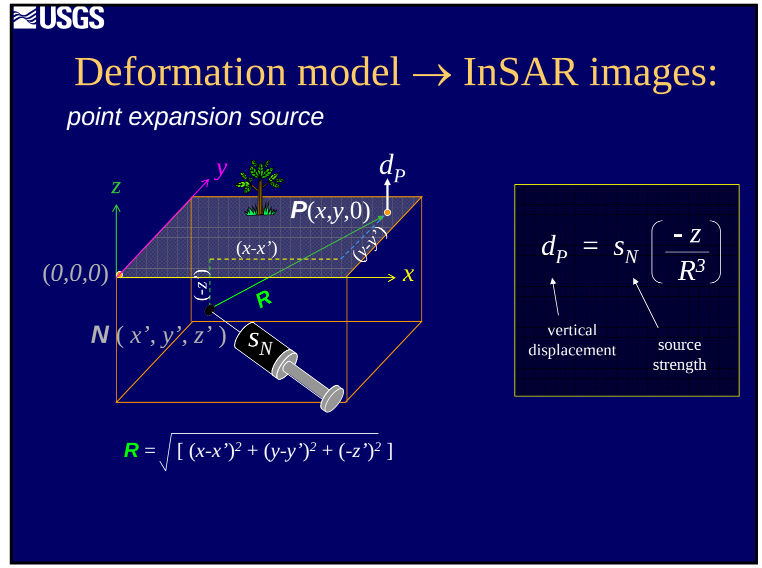
USGS
Deformation model → InSAR images:
point expansion source
z
y
x
d_P
P(x,y,0)
(0,0,0)
(x-x')
(y-y')
(-z')
R
N (x', y', z')
s_N
R = √[(x-x')² + (y-y')² + (-z')²]
$d_P = s_N \left(\frac{-z}{R^3} \right)$
vertical displacement
source strength

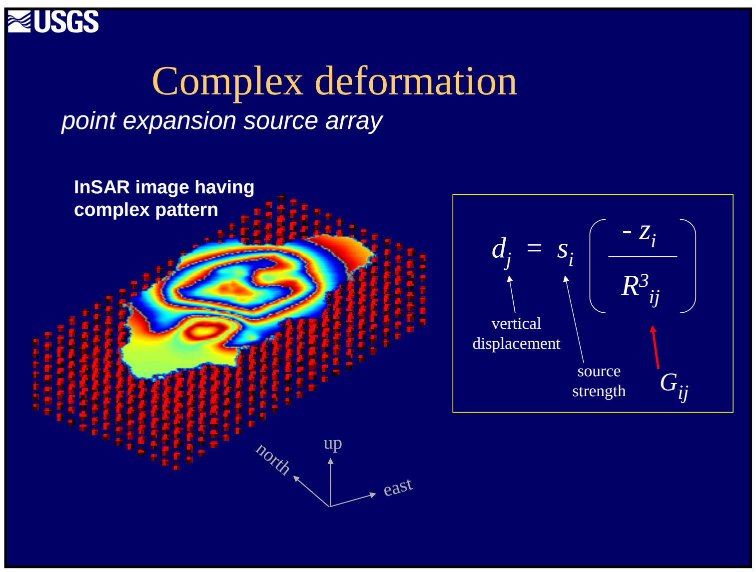
USGS
Complex deformation
point expansion source array
InSAR image having complex pattern
up
north
east
$d_j = s_i \left(\frac{-z_i}{R^3_{ij}} \right)$
vertical displacement
source strength
G_{ij}

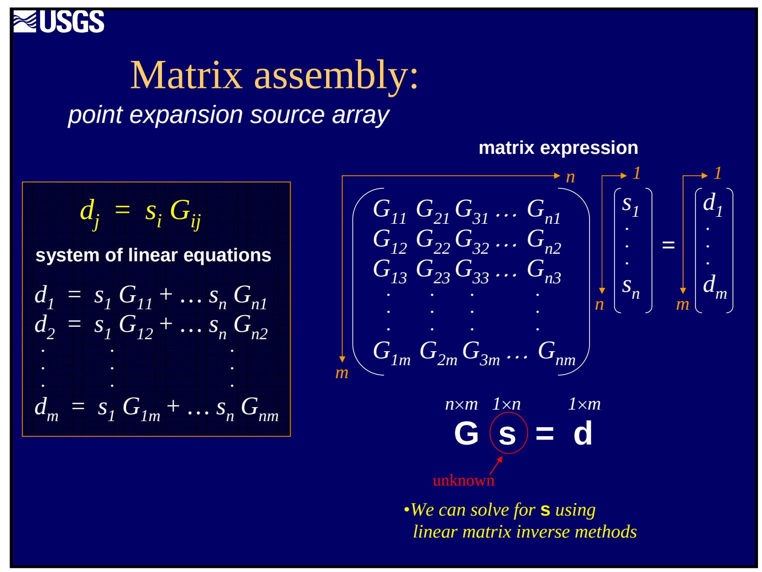
USGS
Matrix assembly:
point expansion source array
$d_j = s_i G_{ij}$
system of linear equations
$d_1 = s_1 G_{11} + \dots s_n G_{n1}$
$d_2 = s_1 G_{12} + \dots s_n G_{n2}$
$d_m = s_1 G_{1m} + \dots s_n G_{nm}$
matrix expression
$G_{11}\ G_{21}\ G_{31} \dots G_{n1}$
$G_{12}\ G_{22}\ G_{32} \dots G_{n2}$
$G_{13}\ G_{23}\ G_{33} \dots G_{n3}$
$G_{1m}\ G_{2m}\ G_{3m} \dots G_{nm}$
$s_1 \dots s_n$
$d_1 \dots d_m$
n×m 1×n 1×m
G s = d
unknown
•We can solve for s using linear matrix inverse methods

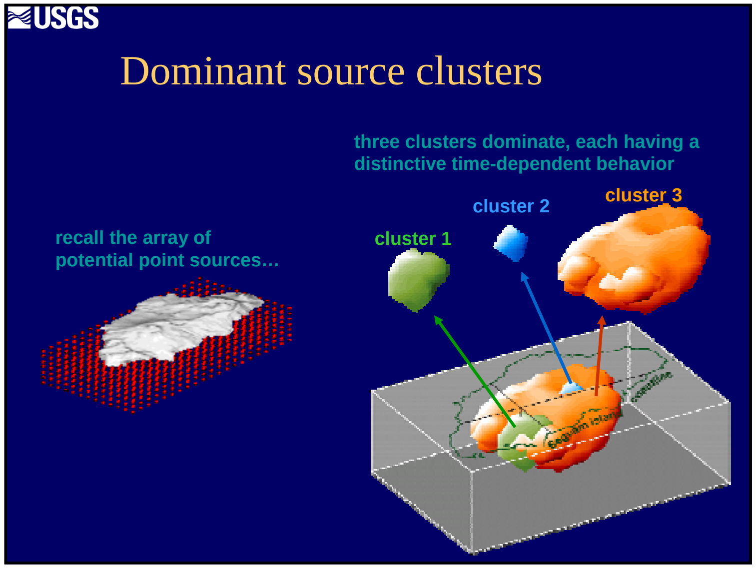
USGS
Dominant source clusters
three clusters dominate, each having a distinctive time-dependent behavior
recall the array of potential point sources...
cluster 1
cluster 2
cluster 3

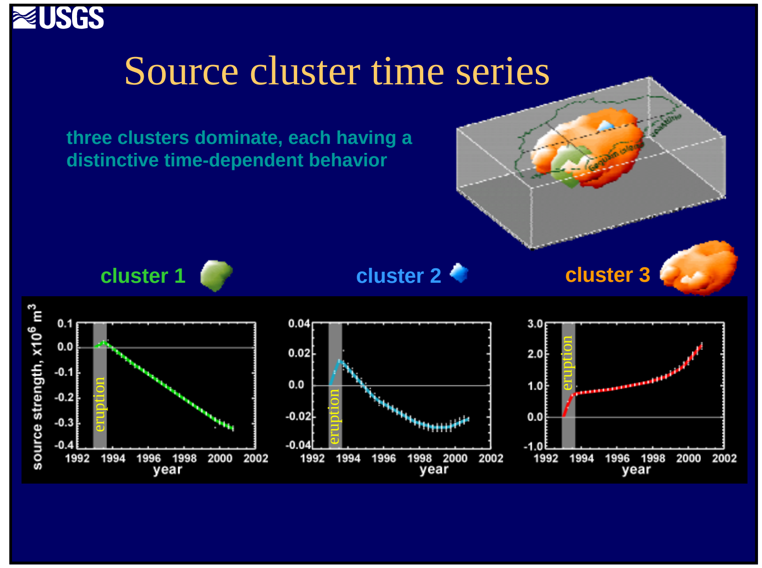
USGS
Source cluster time series
three clusters dominate, each having a distinctive time-dependent behavior
cluster 1
cluster 2
cluster 3
source strength, x10^6 m^3
eruption
year
1992 1994 1996 1998 2000 2002

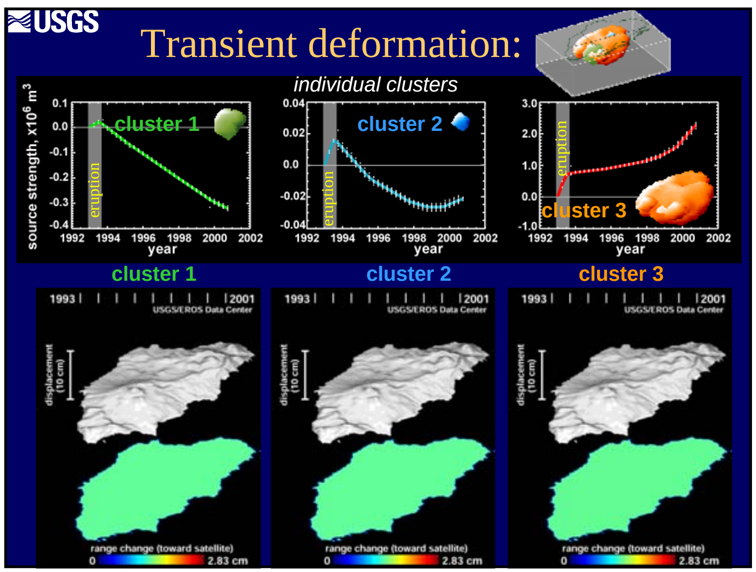
USGS
Transient deformation:
individual clusters
cluster 1
cluster 2
cluster 3
source strength, x10^6 m^3
eruption
year
1992 1994 1996 1998 2000 2002
1993
2001
USGS/EROS Data Center
displacement (10 cm)
range change (toward satellite)
0
2.83 cm

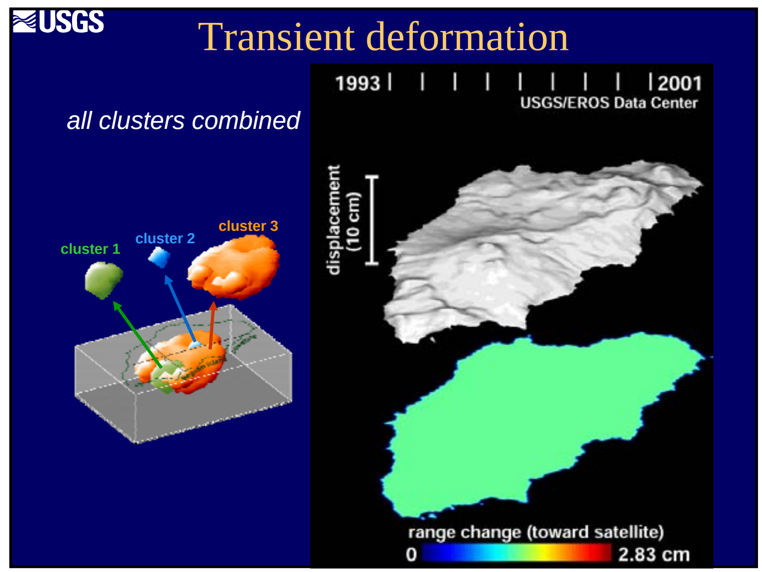
USGS
Transient deformation
all clusters combined
cluster 1
cluster 2
cluster 3
1993
2001
USGS/EROS Data Center
displacement (10 cm)
range change (toward satellite)
0
2.83 cm

USGS

A few thoughts

USGS

Persistent Scatterer InSAR (PSInSAR)

Differential Phase Equation

For pixel *n* in interferogram *i* (corrected for topography):

$$\phi_{n,i} = \phi_{\varepsilon,n,i} + \phi_{defo,n,i} + \phi_{APS,n,i} + \phi_{orbit,n,i} + \sigma_{n,i}$$

DEM Error Term

Deformation in LOS

Atmospheric Phase Term

Orbit Error Term

Noise

USGS

Persistent Scatterer InSAR (PSInSAR)

• PSInSAR uses unique characteristics of atmospheric delay anomalies and backscattering of certain ground targets to improve the accuracy of the conventional InSAR deformation measurement from 1-2 cm to 2-3 mm.

• The basic idea behind PSInSAR is to separate the different phase contributions (surface deformation, atmospheric delay anomaly, and decorrelation noise) by means of least mean square estimation, taking into account the spatio-temporal data distribution and the correlation between the point target samples which have unique SAR backscattering characteristics.

• In urban areas most of the point targets correspond to single buildings or other stable structures. These points can be used as a “natural benchmark” to monitor terrain motion by analyzing the phase history of each target in the image.

USGS

USGS

Conventional InSAR

PS InSAR

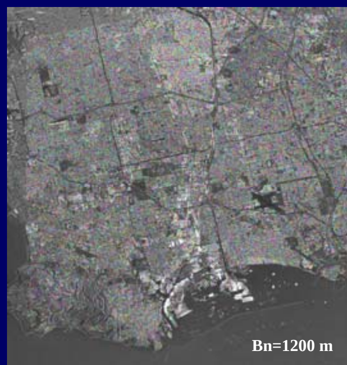

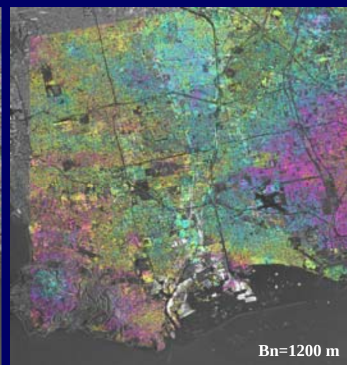

Long Beach, CA

USGS

Average annual deformation over Long Beach, CA

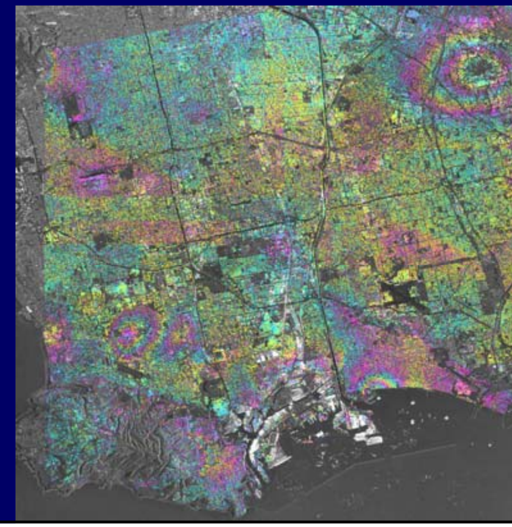

USGS

Atmospheric artifacts in conventional InSAR images are removed using PSInSAR

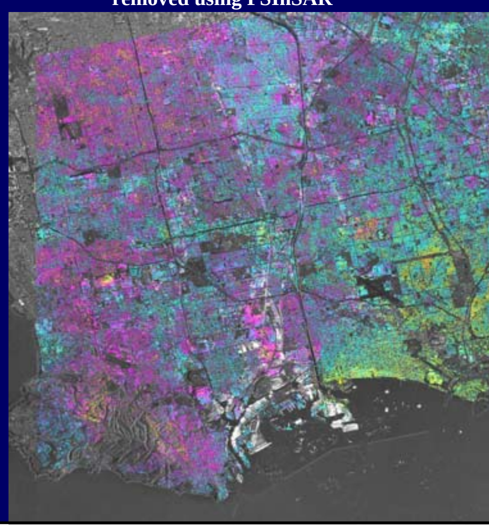

USGS

Deformation history for each point target can now be analyzed using PSInSAR

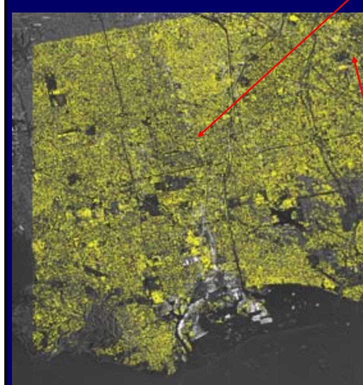

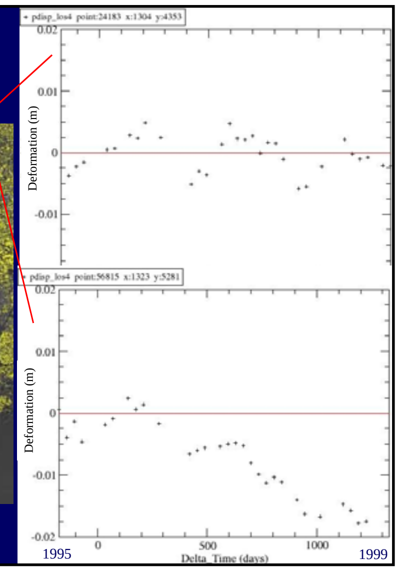

USGS

InSAR Future: from research to operation

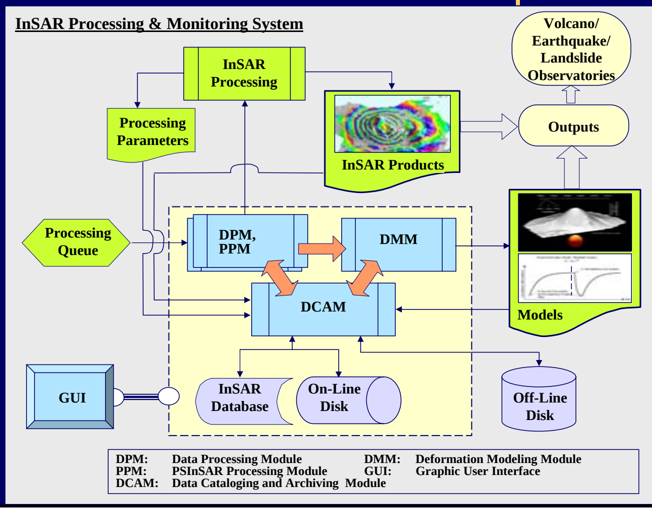

USGS

InSAR Volcano Deformation Monitoring System

GUI-based / Database-driven automated InSAR processing

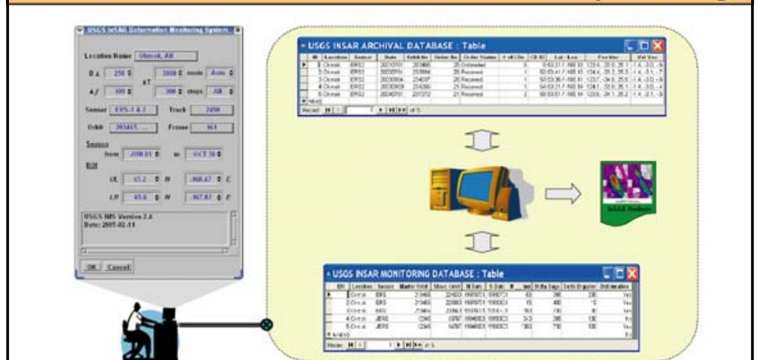

USGS

- **New SAR technologies**
  - **Polarimetric InSAR – biomass mapping**
  - **Permanent Scatters InSAR – measuring deformation at millimeter accuracy**
  - **ScanSAR InSAR – improve spatial and temporal coverage**

- **Applications**
  - **InSAR monitoring of volcano, earthquake, and landslide processes**
  - **Landslide movement with artificial, active radar reflectors**
  - **Sensor fusion: different wavelength/polarization SAR data, LIDAR, optical images**
  - **Mapping biomass with fully polarized SAR and InSAR imagery**
  - **Detecting deformation beneath vegetation with polarimetric InSAR**
  - **Mapping soil moisture at a spatial resolution not achievable from optical imagery**
  - **An automated InSAR processing system**

USGS

Thank you for your attention!